

DETERMINATION OF THE FRESNEL REFLECTION COEFFICIENT OF A HALF-SPACE FOR MEDIUM ESTIMATION PURPOSES

R. Solimene

Department of Information Engineering
Second University of Naples, Via Roma 29, Aversa I-81031, Italy

F. Soldovieri

Institute for Electromagnetic Sensing and of the Environment
National Research Council, Via Diocleziano 328, Napoli I-80124, Italy

A. D'Alterio

Department of Information Engineering
Second University of Naples, Via Roma 29, Aversa I-81031, Italy

Abstract—A novel procedure for estimating the Fresnel reflection coefficient of a transversally homogeneous half-space medium is introduced. GPR multistatic measurements are exploited as data whereas the Fresnel coefficient (as a function of the incidence angle) is retrieved by inverting a linear integral equation. Having estimated the reflection coefficient it can be exploited to determine the medium electromagnetic parameters. Numerical examples are used to show the procedure effectiveness for different types of homogeneous half-space media within a two-dimensional scalar geometry. The case of a layered half-space is also discussed.

1. INTRODUCTION

Determining the electromagnetic properties of a half-space medium is a relevant problem in a number of applicative contexts. For example, in GPR (Ground Penetrating Radar), the knowledge of medium is necessary for subsurface imaging to obtain properly focused images [1]. More in general, the medium estimation problem has been largely dealt

with in the scientific literature. In particular, two main classes of methods for the dielectric permittivity material characterization can be identified. The first one is based on transmission and/or reflection coefficient measurements of material samples allocated, for instance, in wave-guide [2–4]. The other class of techniques, of major interest for this work, is based on the measurement of the reflection/transmission coefficients in free space conditions [5–10] mainly under plane wave incidence assumption.

Here, we eliminate the requirement of free space measurements by taking into account the spatial spectrum of the incident field and by adopting a multistatic scheme to collect data.

More in detail, the estimation of the Fresnel coefficient is cast as the inversion of a linear integral equation. Such an inversion is “stably” achieved through a truncated singular value decomposition (TSVD) scheme. At this juncture, the reflection coefficient is obtained as a function of the angle of incidence. Therefore, view diversity (instead of or jointly to the more usual multi-frequency data) can be exploited for the medium estimation. This last step can be accomplished by a simple algebraic relationship for a homogeneous half-space.

This approach exhibits similarities with the one presented in [11] where the complex effective permittivity of a corrugated slab is determined by comparing the measured and the theoretical reflection/transmission coefficients as the incidence direction of a plane wave varies.

The approach has been already introduced in [12, 13]. There, the method was numerically checked against a very restricted number of cases. In this contribution, we mean to extend the analysis in order to better assess the achievable performance. Therefore, the novel contributions of the present paper, as compared to [12], can be summarized as follows. To give a more complete analysis of the approach by investigating its performances for a broader class of half-space media, including the case where a buried scatterer is present. To study the role of noise and of the measurement line extent. Finally, a more rigorous mathematical formulation supports the entire discussion. In particular, analytical arguments allow to solve the problem of the truncation index choice in the TSVD procedure, the latter being a critical question affecting the trade-off between accuracy and stability against the noise.

We also address the case of a layered half-space. We show that the procedure for reflection coefficient retrieving works also for this case. However, unlike the case of a homogeneous half-space, medium parameters cannot be estimated (starting from the reflection coefficient) simply by means of an algebraic relationship. In this case,

one has to tackle problems related to non-linear optimization which are indeed common to other estimation methods present in literature.

The paper is organised as follows. In Section 2 the considered scattering scenario is described. In Section 3 the estimation procedure is presented. Its numerical analysis is presented in Section 4. Finally, discussion and conclusions end the paper.

2. SCATTERING SCENARIO

We refer to the two-dimensional scalar geometry depicted in Fig. 1. Two homogeneous half-spaces (the case of more than two layers is briefly discussed in the sequel) separated by a planar interface (the air/medium interface located at $z = 0$) are considered. The upper layer is the free-space with dielectric permittivity ϵ_0 and magnetic permeability μ_0 , respectively. The lower half-space can be dispersive and contain ohmic losses σ_S . Therefore, by assuming $\exp(j\omega t)$ time-harmonic convention, its equivalent dielectric permittivity is given as $\epsilon_{EQ}(\omega) = \epsilon_S(\omega) - j\sigma_S/\omega$ with $\epsilon_S(\omega) = \epsilon_{SR}(\omega) - j\epsilon_{SI}(\omega)$.

A multistatic/multiview measurement configuration is considered. That is, for each transmitting positions the field reflected back by the air/medium interface is collected over a set of different positions. The receiving as well as the transmitting positions are taken at the same height from the air/medium interface over an aperture Σ synthesized along the x -axis parallel to and at distance d from the air/medium interface (see Fig. 1). In particular, the antennas are assumed to be two-dimensional sources and far enough from the air/medium interface so that they work as if they were in the free-space.

Moreover, antenna radiation properties are assumed known, for example, by means of a preliminary characterization stage through experiments and/or numerical analyses [14].

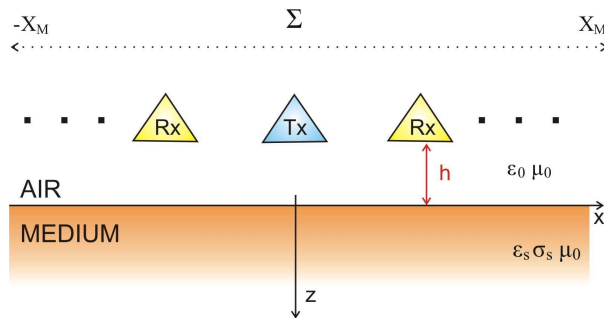


Figure 1. Geometry of the problem.

3. ESTIMATION PROCEDURE

For the scattering scene described above, the field radiated by a two-dimensional antenna, E_{inc} , can be conveniently expressed in terms of its plane-wave spectrum as follows

$$E_{inc}(\underline{r}, \underline{r}_S, k_0) = \int_{-k_0}^{k_0} A(k_0, k_x) \exp(-jk_z|z - z_S|) \exp[-jk_x(x - x_S)] dk_x \quad (1)$$

where $\underline{r} = (x, z)$ is the generic point on the air/medium interface and $\underline{r}_S = (x_S, z_S)$ is the transmitting antenna position. $A(k_0, k_x)$ is the source plane-wave spectrum, k_0 is the free-space wave-number and $k_z = \sqrt{k_0^2 - k_x^2}$. Note that, as we are considering antennas not in close proximity of the air/medium interface, evanescent waves have been neglected in Eq. (1). Moreover, as the incident field is linearly polarized along the y -axis we are actually considering a TE_z case.

Accordingly, the field reflected back by the interface, E_R , can be expressed as

$$E_R(x_O, x_S, k_0) = \int_{-k_0}^{k_0} A(k_0, k_x) \exp(-2jk_z d) \exp[-jk_x(x_O - x_S)] \Gamma(k_0, k_x) dk_x \quad (2)$$

where $\underline{r}_O = (x_O, -d)$ and $\underline{r}_S = (x_S, -d)$ are the observation and the source positions, and $\Gamma(k_0, k_x)$ is the Fresnel reflection coefficient at the air/medium interface.

Equation (2) establishes a relationship between the field measurements and the reflection coefficient which, in turn, depends on the electromagnetic parameters of the investigated medium. This suggests the adoption of a two-step based estimation procedure. First, Eq. (2) is solved for $\Gamma(k_0, k_x)$. Then, $\varepsilon_{EQ}(\omega)$ can be estimated starting from the retrieved reflection coefficient.

These two steps are detailed below.

3.1. Reflection Coefficient Retrieving

As to the first step, since both E_R and Γ depend on the frequency (through the wave-number k_0) this requires solving Eq. (2) separately for each adopted frequency.

Let us denote by $k_{01}, k_{02}, \dots, k_{0N}$ the free-space wave-numbers corresponding to N frequencies taken within the frequency band $[k_{0\min}, k_{0\max}]$.

Then, Eq. (2) at the h -th frequency ($h \in (1, 2, \dots, N)$) can be written as

$$E_R(x_O, x_S, k_{0h}) = \int_{-k_{0h}}^{k_{0h}} A(k_{0h}, k_x) \exp(-2jk_zhd) \exp[-jk_x(x_O - x_S)] \Gamma(k_{0h}, k_x) dk_x \quad (3)$$

Accordingly, the first step of the estimation procedure consists in solving Eq. (3) for $\Gamma(k_{0h}, k_x)$ in correspondence to a collection of N frequencies. To this end, we conveniently rewrite Eq. (3) as

$$E_R(\eta, k_{0h}) = (A_h \Gamma)(\eta, k_{0h}) = \int_{-k_{0h}}^{k_{0h}} A(k_{0h}, k_x) \exp(-2jk_zhd) \exp(-jk_x\eta) \Gamma(k_{0h}, k_x) dk_x \quad (4)$$

where we have now considered $\eta = x_O - x_S$ as the observation variable. Moreover, for future convenience, in Eq. (4) we also reported operator notation, A_h (subscript h once again is a reminder that we are working at the single h -th frequency), of the involved integral operator.

At this stage, one realizes that multi-monostatic or multi-bistatic configurations cannot be exploited to invert Eq. (4). Indeed, for such configurations η would assume a single fixed value which would entail solving Eq. (4) by exploiting a single data. Therefore, we conclude that multistatic and/or multi-view/multistatic configurations are required to solve the inverse problem at hand.

In order to obtain a reliable and effective (from the computational point of view) inversion procedure, the mathematical features of the linear operator in Eq. (4) have to be investigated and taken into account.

First, we need to specify the functional sets to which data E_R belong to and where the unknown Γ is searched for. To this end, we assume $E_R \in L^2[-\eta_{\max}, \eta_{\max}]$, that is the set of square integrable functions defined over $[-\eta_{\max}, \eta_{\max}]$ (η_{\max} being equal to $2X_M$ since $x_O, x_S \in \Sigma = [-X_M, X_M]$), and $\Gamma \in L^2[-k_{0h}, k_{0h}]$. Moreover, it is easy to see that the operator in Eq. (4) being of Hilbert-Schmidt class is indeed compact [15]. This entails that, in order to have a meaningful solution, some regularization scheme must be applied. To address this issue the Singular Value Decomposition (SVD) of Eq. (4) is exploited. Indeed, the singular system $\{u_{hn}, v_{hn}, \sigma_{hn}\}_{n=0}^{\infty}$ of the operator (4) provides a way to implement the inversion scheme and, what is more, allows to gather information on how to regularize the inverse problem and to sample (in the spatial domain) the reflected

field data. More in detail, the singular functions u_{hn} and v_{hn} are the eigenfunctions of $A_h^* A_h$ and of $A_h A_h^*$ (A_h^* being the adjoint of A_h), respectively, associated with the same eigenvalue σ_{hn}^2 . Then, the u_{hn} form an orthonormal basis in the space of unknowns while the v_{hn} form an orthonormal basis in the data space. Moreover, they are a solution of the following shifted eigenvalue problem [15]

$$A_h u_{hn} = \sigma_{hn} v_{hn}, \quad A_h^* v_{hn} = \sigma_{hn} u_{hn} \quad (5)$$

Accordingly, the least square generalized solution at the single h -frequency, $\tilde{\Gamma}(k_{0h}, k_x)$, can be expressed as

$$\tilde{\Gamma}(k_{0h}, k_x) = \sum_{n=0}^{\infty} \frac{\langle E_R(k_{0h}, \eta), v_{hn}(\eta) \rangle_Y}{\sigma_{hn}} u_{hn}(k_x) \quad (6)$$

where $\langle \cdot, \cdot \rangle$ denotes the scalar product in the data functional space $L^2[-\eta_{\max}, \eta_{\max}]$. In particular, as the operator at hand is a compactly supported Fourier transform operator, its image (i.e., the corresponding reflected field) can vanish only when the function $A(k_{0h}, k_x)\Gamma(k_{0h}, k_x)$ is identically zero within $[-k_{0h}, k_{0h}]$. The occurrence of the latter circumstance is unlikely. Therefore, it can be concluded that the operator in Eq. (4) is injective and hence $\tilde{\Gamma}(k_{0h}, k_x)$ coincides with $\Gamma(k_{0h}, k_x)$ in the case of noise-free data.

Unfortunately, due to the compactness of the operator at hand, its singular values cluster to zero as their index increases. Therefore, in order to obtain a stable solution (against noise and uncertainties), series in Eq. (6) must be truncated. This leads to a TSVD inversion [15], that is

$$\tilde{\Gamma}(k_{0h}, k_x) = \sum_{n=0}^{N_{Th}} \frac{\langle E_R(k_{0h}, \eta), v_{hn}(\eta) \rangle}{\sigma_{hn}} u_{hn}(k_x) \quad (7)$$

where we once again adopted $\tilde{\Gamma}(k_{0h}, k_x)$ to denote the TSVD-regularized reconstruction and N_{Th} is the truncation index. The key point, now, is the choice of the truncation N_{Th} which dictates the compromise between accuracy and stability.

To this end, we introduce the auxiliary operator B_h defined as follows

$$B_h \Gamma = \int_{-k_{0h}}^{k_{0h}} \max |A(k_{0h}, k_x)| \exp(-2jk_z h d) \exp(-jk_x \eta) \Gamma(k_{0h}, k_x) dk_x \quad (8)$$

where $\max |A(k_{0h}, k_x)|$ picks up the maximum of the amplitude of $A(k_{0h}, k_x)$.

It can be easily proven that

$$\|A_h g\| \leq \|B_h g\| \quad \forall g \in L^2([-k_{0h}, k_{0h}]) \quad (9)$$

where $\|\cdot\|$ denotes the standard L^2 norm in the data space. Eq. (9) entails that

$$\sigma_{hn} \leq \sigma_n(B_h) \quad \forall n \quad (10)$$

where $\sigma_n(B_h)$ are the singular values of B_h .

Therefore, the singular values of B_h are larger than those of A_h . Moreover, as the singular system of operator B_h is related to the prolate spheroidal functions [16], its singular values have a step-like behaviour with the knee occurring at the index $[2\eta_{\max}k_{0h}/\pi]$, $[\cdot]$ denoting the integer part operator. Thus, by virtue of Eq. (10), we conclude that an upper bound for the truncation index in Eq. (7) is $N_{Th} = [2\eta_{\max}k_{0h}/\pi]$. A lower bound can be estimated by following the theory developed in [17]. However, if a source with a broad plane-wave spectrum is considered (non directive antennas are in general also useful for imaging purposes as they allow to form a large synthetic aperture), the previous estimation works well. Properties of the prolate spheroidal functions can be also exploited to derive the sampling step while collecting data [16]. Accordingly, the previous estimation for the truncation index N_{Th} also gives the number of required data.

In the following examples, while the truncation index in Eq. (7) is chosen according to the previous discussion, that is varying according to frequency, the number of measurements in the η domain is fixed and chosen in correspondence to the highest adopted frequency, that is $N_{TN} = [2\eta_{\max}k_{0N}/\pi]$.

Finally, we remark that the implementation of Eq. (7) requires discretizing Eq. (4). To this end, a standard method of moment is employed by adopting a finite dimensional representation for $E_R(\cdot)$ and $\Gamma(\cdot)$. In particular, delta functions are adopted to discretize the unknown whereas a point matching procedure (over N_{TN} points for the η variable in correspondence to each adopted frequency) is imposed in the data domain. Accordingly, the discretized counterpart of Eq. (4) becomes

$$\mathbf{E}_R = \mathbf{A}_h \Gamma \quad (11)$$

where \mathbf{E}_R and Γ are vectors representing the collected reflected field data and the discretized version of the unknown, respectively, and \mathbf{A}_h is a matrix representing the discretized linear operator in (4). Afterwards, the singular system of \mathbf{A}_h is numerically computed and used to implement Eq. (7).

3.2. Determining the Medium's Parameters

The inversion of Eq. (4) provides an estimation of the Fresnel reflection coefficient, $\tilde{\Gamma}(k_{0h}, k_x)$, as a function of the spectral (angular) variable k_x at each working frequency. At this stage, the working hypothesis about the investigated medium as homogeneous half-space is not entered yet. Indeed, the procedure presented is quite general and requires only the homogeneity of the medium along the x -axis.

When the investigated medium is a homogeneous half-space, the equivalent dielectric permittivity can be directly derived from the reflection coefficient via an algebraic mathematical relationship as

$$\tilde{\varepsilon}_{EQ}(\omega_h) = \frac{k_x^2 + k_z^2 \left\{ \left[1 - \tilde{\Gamma}(k_{0h}, k_x) \right] / \left[1 + \tilde{\Gamma}(k_{0h}, k_x) \right] \right\}^2}{\omega_h^2 \mu_0} \quad (12)$$

where ω_h is the h -th adopted angular frequency.

In the ideal case of noise and uncertainties free data, regularization would not be necessary and Eq. (12) would return an $\tilde{\varepsilon}_{EQ}(\omega_h)$ which does not depend on the spectral variable k_x . However, due to the necessity of adopting the TSVD scheme in order to mitigate the effect of the model error and the noise, the dielectric permittivity becomes a function of k_x , that is $\tilde{\varepsilon}_{EQ}(\omega_h, k_x)$. Therefore, as the reflection coefficient is recovered for all the $k_x \in [-k_{0h}, k_{0h}]$, the dielectric permittivity can be estimated by averaging $\tilde{\varepsilon}_{EQ}(\omega_h, k_x)$ over k_x . Accordingly, at the h -th frequency we obtain

$$\tilde{\varepsilon}_{EQAV}(\omega_h) = \frac{1}{2\alpha k_{0h}} \int_{-\alpha k_{0h}}^{\alpha k_{0h}} \tilde{\varepsilon}_{EQ}(\omega_h, k_x) dk_x \quad (13)$$

where the factor $\alpha < 1$ is used to mitigate the loss of accuracy in the reflection coefficient reconstruction at the edges of the integration domain. The averaging procedure in Eq. (13) is also useful in curtailing the effect of the residual noise after the application of the TSVD scheme.

When the half-space is a layered medium, estimating the equivalent dielectric permittivity from the retrieved reflection coefficient becomes a much more difficult task. In this case, it is generally required to run an optimization algorithm for identifying the medium parameters. However, the proposed procedure can be useful as it gives a further degree of freedom in tackling such a problem. Indeed, the knowledge of the reflection coefficient as a function of the angle of incidence, besides the more usual multi-frequency data, can be exploited to estimate the medium parameters.

4. NUMERICAL RESULTS

This section reports some numerical results with the aim of assessing the performances of the proposed estimation procedure. To this end, synthetic data have been generated simply by numerically implementing Eq. (2) and extending the integration domain slightly beyond the visible spectrum. The reflected field is collected over an aperture $\Sigma = [-X_M, X_M]$ synthesized at a height $d = 0.2$ m above the air/medium interface. Two different transmitting antenna positions located at the edges of the aperture, that is at $x_S = -X_M$ and $x_S = X_M$, are employed. This allows the observation variable $\eta = x_O - x_S$ to range within the observation interval $[-2X_M, 2X_M]$. $N = 15$ frequencies taken uniformly within the frequency band $[0.3, 1]$ GHz are considered. Hence, according to the discussion reported in the previous section, for all the frequencies $N_{TN} = [2\eta_{\max}k_{0N}/\pi]$ data samples are employed for the reflection coefficient retrieving.

As to the source plane-wave spectrum, we assume that

$$A(k_x) = \cos(0.1k_x/2) / [1 - (0.1k_x/\pi)^2] \quad (14)$$

which resembles the one of a horn-antenna. Finally, in the averaging procedure of Eq. (13), the edge factor α is chosen equal to 0.7.

4.1. Homogeneous Half-space

We first consider a homogeneous half-space. In particular, we start by considering the case of a lossless medium in order to study how the estimation capability of the proposed method depends on the dielectric permittivity of the medium and on the noise. To this end, we assume to collect the data over an aperture with $X_M = 1$ m (this entails considering fourteen equally spaced, over Σ , measurement points for each source position and for each frequency) and consider three different values of the relative dielectric permittivity (4, 9 and 18) representative of a clay dry, a permafrost and a sand wet materials, respectively [18]. The corresponding estimation results are reported in Fig. 2. In that figure, the actual and the estimated relative dielectric permittivity profiles (as a function of the frequency) are compared for noise free and noisy data. The maximum (over the frequency band) relative discrepancy, that is $e_r = \max[(\tilde{\varepsilon}_{EQAV}(f)/\varepsilon_0 - \varepsilon_{EQ}(f)/\varepsilon_0) / (\varepsilon_{EQ}(f)/\varepsilon_0)]$ (note that for the example at hand ε_{EQ} does not depend on the frequency), is employed to quantify the estimation quality.

Moreover, e_{rN} is the same as e_r but refers to the case of data corrupted by noise. In particular, we considered a zero mean additive complex white Gaussian noise with the signal to noise ratio (SNR)

given in the figures. As can be seen, the estimation procedure works very well in absence of noise. However, it can be also noted that the estimation accuracy degrades with noisy data, especially for the case of the medium with the highest value of dielectric permittivity (bottom panel of Fig. 2).

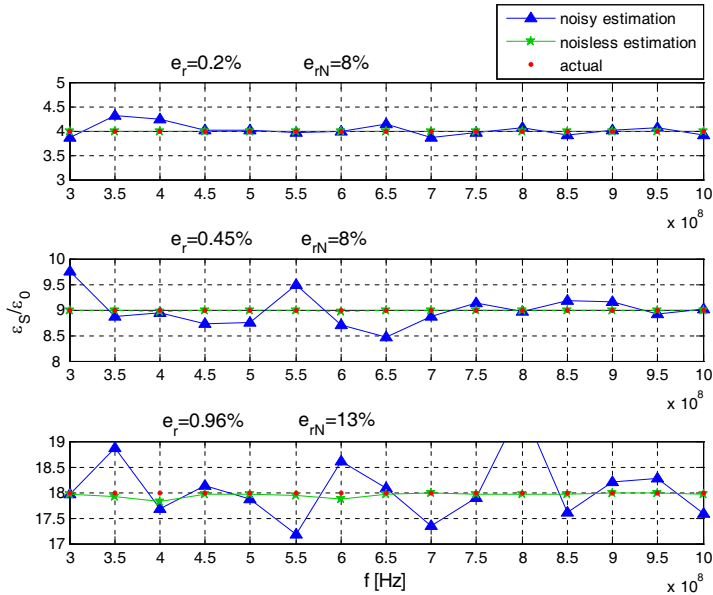


Figure 2. Estimation results for lossless media (SNR = 15 dB).

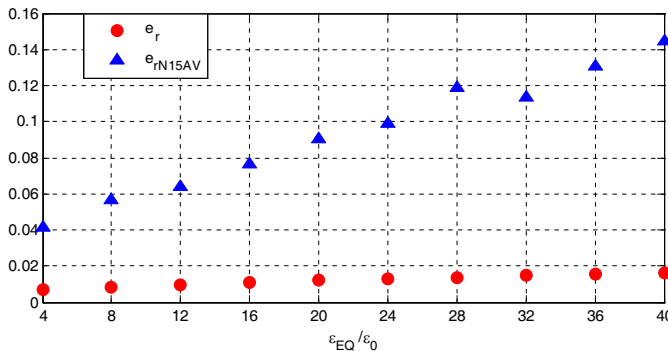


Figure 3. Illustrating the role of the dielectric permittivity (for lossless media) on the estimation procedure.

In order to further investigate about the role of the dielectric permittivity, in Fig. 3, we analyze the estimation performance for a larger interval of $\varepsilon_{EQ}/\varepsilon_0$ which ranges from 4 to 40 with a step of 4 [18]. In particular, in that figure we report e_r and e_{rN15AV} , the latter being e_{rN} averaged over 100 different noise realizations with the SNR equals to 15 dB. As can be seen, according to the previous examples, the estimation gets worse as the dielectric permittivity increases.

In Fig. 4, we turn to consider the role of the measurement aperture in conjunction to the case of $\varepsilon_{EQ} = 18\varepsilon_0$. To this end, the measurement aperture is enlarged to $X_M = 2$ m (thus, the observation domain and the number of measurement points are doubled compared to the previous case). As can be seen, all the error figures improve. This shows how the increase in the extent of the measurement aperture favorably affects the estimation procedure. This can be easily explained by recalling Eq. (4) from which one can deduce that a larger measurement aperture entails a less severe filtering while reconstructing the reflection coefficient via the regularization scheme. The improvement is also observed for noisy data. For this case, we also increased the SNR passing from 15 dB to 25 dB. The corresponding error figure, denoted by e_{rN25} , returned a value of 0.8% which is very close to the noiseless case. We also considered the averaged error figure which practically returned the same value.

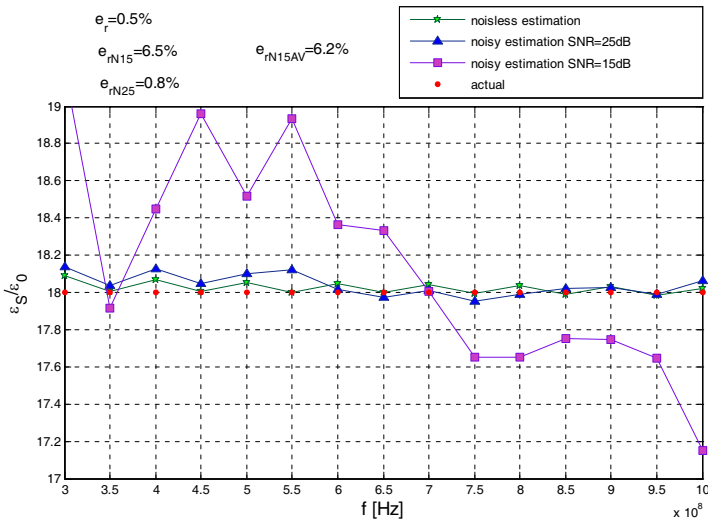


Figure 4. The same case as at the bottom of Fig. 2 with the measurement aperture doubled in extent $X_M = 2$ m.

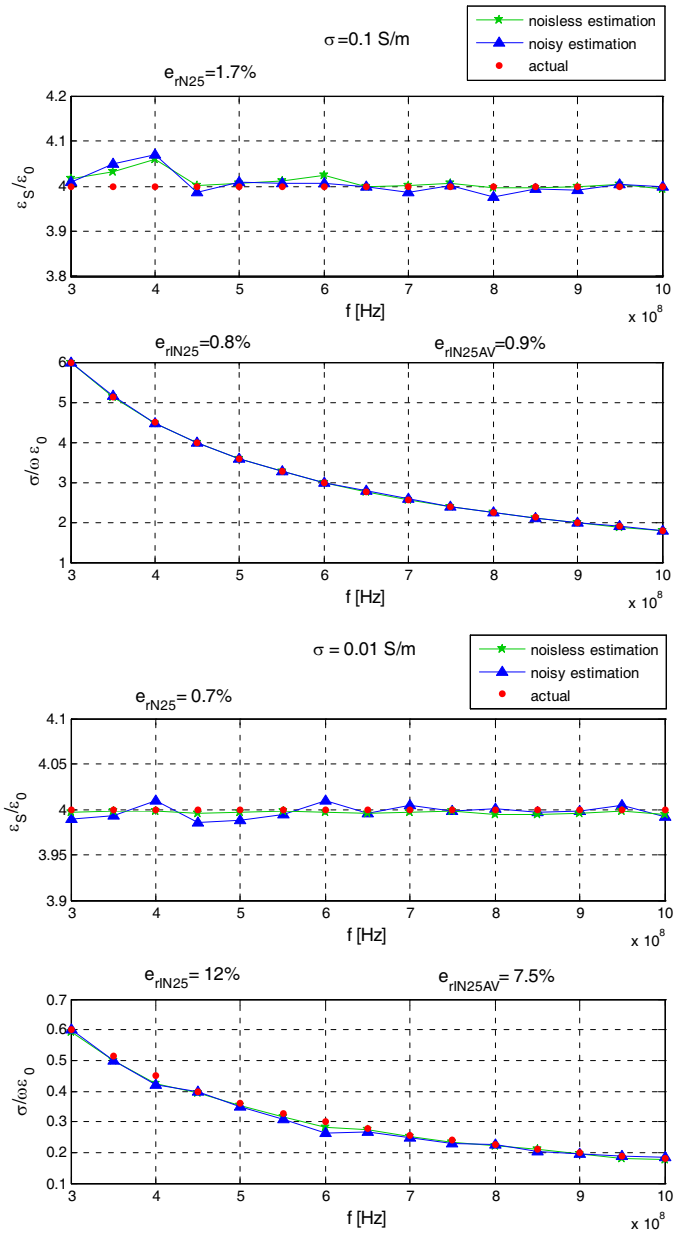


Figure 5. Estimation of an ohmic lossy medium. The configuration is the same as in Fig. 2 with $\text{SNR} = 25$ dB.

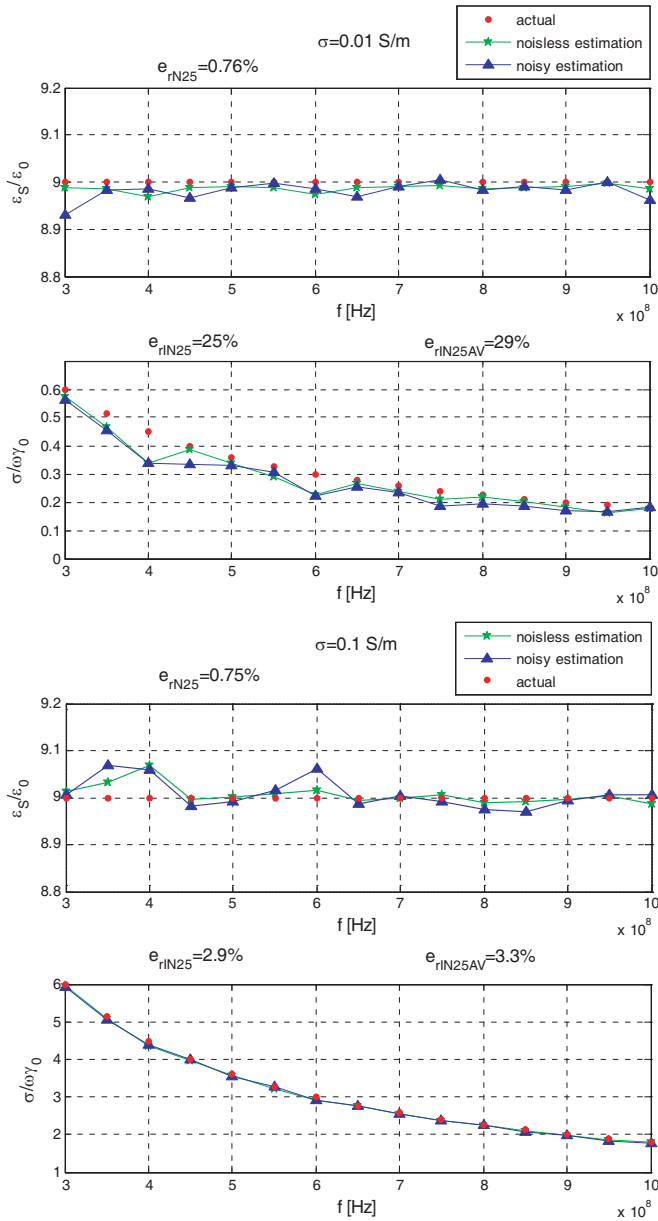


Figure 6. The same as in Fig. 5 but with an increased medium dielectric permittivity.

We turn now to address the case of a medium containing conductive losses as well (see Fig. 5) so that $\varepsilon_{EQ}(\omega) = \varepsilon_S - j\sigma_S/\omega$, with $\varepsilon_S = 4\varepsilon_0$. Two different values of the electric conductivity, $\sigma_S = 0.01\text{ S/m}$ and $\sigma_S = 0.1\text{ S/m}$ are considered and the same measurement configuration as the one adopted for Fig. 2 is exploited ($X_M = 1\text{ m}$). The noiseless estimations practically coincide with the actual medium parameters hence we quantified only the noisy estimation (SNR = 25 dB). As can be seen, for both the cases the real part of $\varepsilon_{EQ}(\omega)$ is well estimated (e_{rN25} returns 0.7% and 1.7%, respectively) and the error figure gives results comparable to those obtained in the lossless case. This means that the presence of the conductivity σ_S , at least for the value up to 0.1 S/m, does not significantly affect the estimation of the real part of $\varepsilon_{EQ}(\omega)$. As to the imaginary part of $\varepsilon_{EQ}(\omega)$, by looking at the corresponding error figures (denoted as e_{rIN25} and $e_{rIN25AV}$) it can be noted that the lower σ_S the worse the estimation. This, of course, is to be expected. Indeed, having fixed the SNR, the noise contribution in the estimation does not depend on the unknown and clearly corrupts the reconstruction of the lower unknown to a larger extent. On the other hand, the SNR is linked to the reflected field norm energy but the latter, for the case

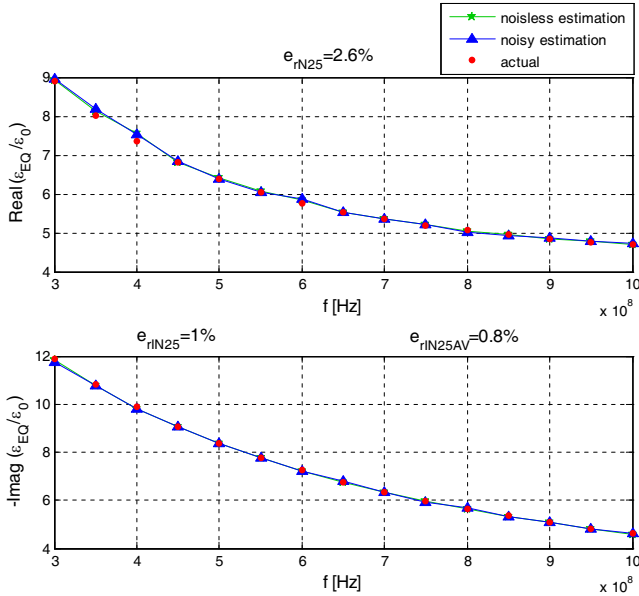


Figure 7. Estimation of a first-order Debye plus conductive losses medium. The measurements parameters are the same as in Fig. 2 with SNR = 25 dB.

at hand, mainly depends on the dielectric permittivity of the medium. This conclusion is furthermore supported by the example reported in Fig. 6 where, by increasing the dielectric permittivity of the medium to $\varepsilon_S = 9\varepsilon_0$, we have that the estimation of the imaginary part of $\varepsilon_{EQ}(\omega)$ degrades. In fact, in this case, as ε_S increased so did the energy norm of the reflected field and hence the noise (having fixed the SNR = 25 dB). In all cases, the estimations are very good and useful for possible subsequent imaging.

The last example we present refers to a medium which accounts for conductive losses as well as dispersive phenomena described in terms of the first order Debye model, that is $\varepsilon_{EQ}(\omega) = \varepsilon_0[\varepsilon_\infty - j\frac{\sigma_S}{\omega\varepsilon_0} + \frac{\varepsilon_{ST}-\varepsilon_\infty}{1+j\omega\tau_e}]$ with $\varepsilon_{ST} = 16$, $\varepsilon_\infty = 4$, $\sigma_S = 0.1$ S/m and $\tau_e = 64$ ns. From Fig. 7, it can be seen that also in this case the estimation procedure works very well with both noise-free and noisy data (SNR = 25 dB).

4.2. Estimation in Presence of Buried Scatterers

In all the previous examples, no scatterers were buried in the medium. This circumstance does not necessarily occur in practical situations. In these cases, the field scattered by possible buried objects acts as a disturb which negatively affects the estimation procedure. Of course, the amount of such a disturbance will depend on the scatterers' characteristics (i.e., location, shape, material composition) and on soil's properties. Therefore, it is useful to check the estimation procedure also in presence of buried scatterers. To this end, we consider a metallic circular cylinder of radius equal to 0.1 m buried relatively close to the interface at a depth of 0.2 m beneath it (i.e., the depth of its center is 0.3 m). In particular, the field scattered by the buried object is computed numerically by solving an electric field integral equation once the proper boundary conditions are forced on its contour. The resulting field is then propagated through the interface by neglecting the mutual scattering between the object and the interface. In order to analyze the role of the scatterer's position relatively to the measurement aperture, four different centre's locations are considered, i.e., $p_1 = (0, 0.3)$ m, $p_2 = (-0.5, 0.3)$ m, $p_3 = (-1, 0.3)$ m and $p_4 = (-1.5, 0.3)$ m. As to the measurement configuration, we maintain $X_M = 1$ m and 15 frequencies taken uniformly within [0.3, 1] GHz. Finally, in order to also examine different soils we consider two cases with $\varepsilon_S = 4\varepsilon_0$, $\sigma_S = 0$ S/m and $\varepsilon_S = 4\varepsilon_0$, $\sigma_S = 0.1$ S/m, respectively. The estimation results corresponding to these cases are reported in Fig. 8. In particular, there, the top panel reports e_r and e_{rN25AV} for the lossless case whereas the bottom panel refers to the lossy case and reports e_r , e_{rI} , e_{rN25AV} and $e_{rIN25AV}$. As expected, when losses are present the estimation is

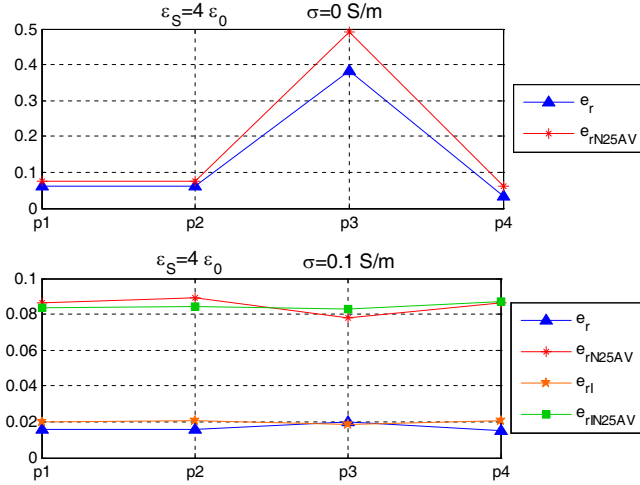


Figure 8. Estimation in presence of a buried scatterer for different scatterer's positions.

relatively immune to the scatterer disturbance as the error is almost constant over the scatterer's positions and comparable to the results obtained previously for the same medium. In the lossless case, instead, the error increases, particularly for the position p_3 (when the scatterer is just in front one of the transmitting antennas). However, as soon as the aperture is slightly slid, so that the object is located in p_4 , the estimation procedure turns to be effective. Therefore, if the measurement aperture is kept small, one can think to slide it over a different portion of the half-space to reduce the disturbance arising from the buried objects.

Finally, we remark that, when the object is more deeply located things get better also in the lossless case.

4.3. Layered Half-space

We end this section by addressing the case of a two-layered half-space. In this case we report results concerning the reflection coefficient estimation only. Starting from the reflection coefficient the medium parameters can be determined by an optimization algorithm but this part is not addressed herein.

We first consider the case of a two-layered lossless half-space (hence, actually the medium has three layers with the upper one being the free-space). The first layer is 13 cm thick with relative dielectric permittivity of $\epsilon_{S1}^r = 4$, whereas the second layer is unbounded and has

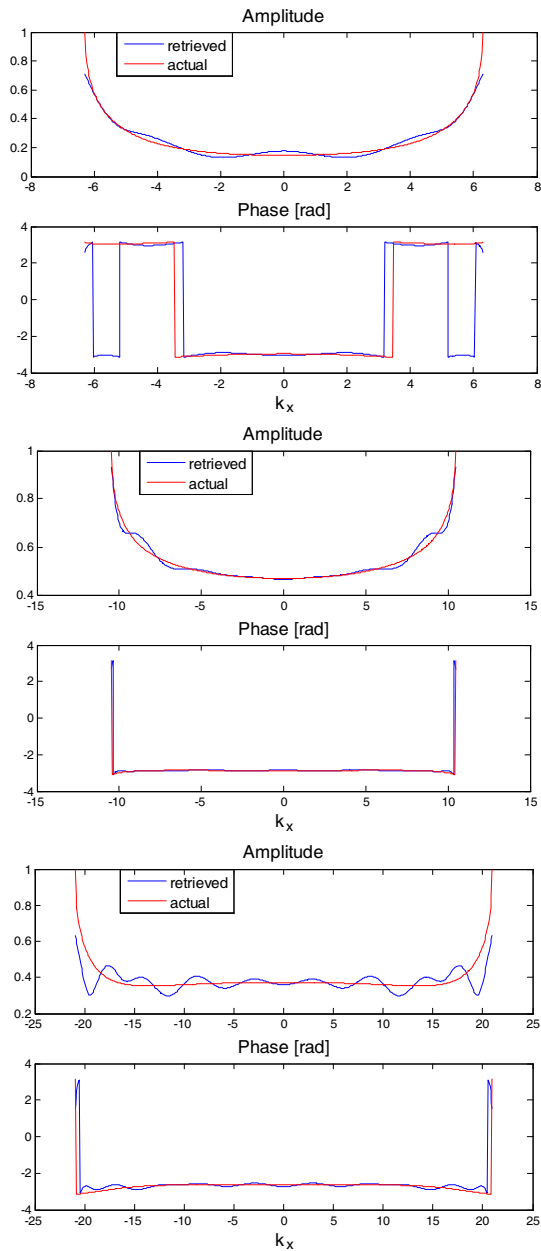


Figure 9. The reflection coefficient in the case of a lossless two-layered half-space medium for $f = 0.3$ GHz (top panel), $f = 0.5$ GHz (middle panel) and $f = 1$ GHz (bottom panel).

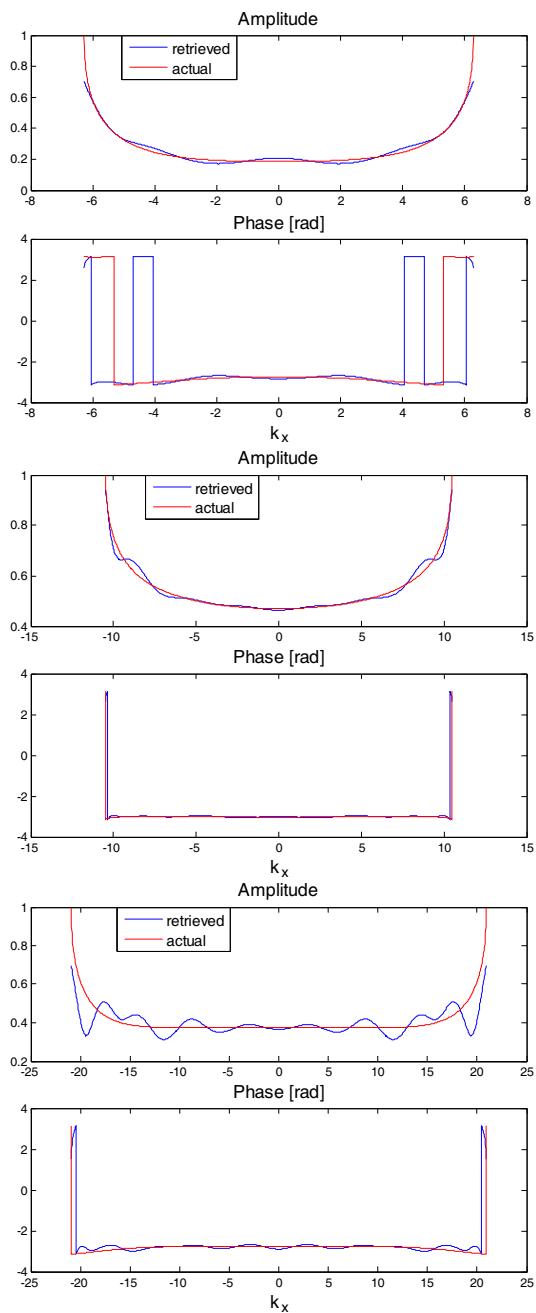


Figure 10. The same as in Fig. 7 but with ohmic losses in the medium.

a relative dielectric permittivity of $\varepsilon_{S2}^r = 9$. For the same measurement set-up as already employed in the previous cases, the corresponding retrieved reflection coefficient is reported in Fig. 9 for three frequencies (i.e., 300 MHz, 500 MHz and 1 GHz) chosen among the adopted fifteen. A further example, where we now added conductivity losses to the medium ($\sigma_{S1} = 0.01 \text{ S/m}$ and $\sigma_{S2} = 0.1 \text{ S/m}$ in the first and the second layer, respectively) is reported in Fig. 10. In both cases, by comparing the estimated reflection coefficient and the actual one, the effect due to the regularization algorithm is well evident. In particular, the typical oscillating behaviour due to the truncation in the TSVD expansion can be appreciated. Moreover, the estimation get worsen at the edge of the k_x domain, especially as to the phase estimation (that is why, while addressing the single-layer half-space medium, we adopted an edge factor in Eq. (13)). Finally, the estimation obtained at 1 GHz appears worse than the other ones. It can be shown that this is because, at that frequency, the filtering introduced by the TSVD is slightly more severe. Notwithstanding, these estimations look like the ones obtained in the case of a single-layer half-space medium (not shown here), hence one can hope to succeed in inferring the medium parameters as before.

In order to assess the quality of the results, the estimated and the actual reflection coefficients should be compared according to some suitable metric. However, having done this, one should be able to propagate such a mismatch on the estimation of the medium parameters. We did not followed this path in the previous examples. Rather, we directly quantified the estimation goodness on the medium parameters. For a layered half-space, this would entail dealing with a non-linear optimization problem. Hence, the achievable performance could be also dependent on the type of optimization algorithm one may want to adopt. In order to obtain a general indication about the quality of the reflection coefficient estimation one can look at a cost functional accounting for the mismatch between the estimated reflection coefficient and the theoretical one, the latter obtained while the medium parameters vary. Accordingly, one can conclude that the reflection coefficient estimation is good when the absolute minimum of such a functional occurs sufficiently close to the actual medium parameters. To follow this approach, we consider the functional defined below

$$\Phi(\underline{m}) = \left\| \Gamma(\underline{m}) - \tilde{\Gamma} \right\|^2 / \max \left\| \Gamma(\underline{m}) - \tilde{\Gamma} \right\|^2 \quad (15)$$

where \underline{m} is a vector containing the parameters of the medium to be searched for, Γ and $\tilde{\Gamma}$ are the stacked vectors (over k_x and k_0) representing the trial and the estimated reflection coefficients and

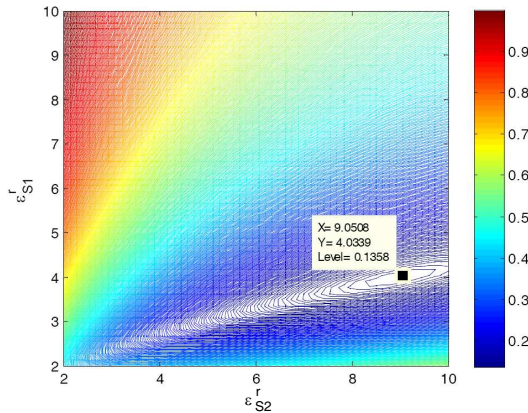


Figure 11. Contour plot of the cost functional of Eq. (15). The reflection coefficient estimations for the case reported in Fig. 9 have been exploited by assuming to know the thickness of the first layer.

the max functional is defined over the interval to which the medium parameters are assumed to belong to.

Figure 11 reports the functional of Eq. (15) built by exploiting the reflection coefficient estimations obtained in the case of Fig. 9. For the sake of convenience of visualization, the functional is displayed as a function of ε_{S1}^r and ε_{S2}^r whereas the thickness of the first layer is assumed equal to the actual one. As can be seen, the absolute minimum just occurs very close to the true medium parameters. Therefore, according to the previous discussion, we can conclude that the reflection coefficient estimation is good.

5. DISCUSSION AND CONCLUSIONS

In this paper, we have addressed the problem of the estimation of the equivalent dielectric permittivity of a homogeneous half-space medium starting from GPR surface measurements. The problem is of interest not only for medium characterization but also for subsurface imaging. In this context, in fact, a preliminary medium characterization allows to mitigate air/medium clutter and is mandatory to correctly form subsurface images.

A simple procedure based on the retrieving of the Fresnel reflection coefficient accounting for the reflection occurring at the air/medium interface has been presented and checked against synthetic noisy data. Both the cases of conductive and dispersive half-spaces have been considered. It is shown that the procedure gives satisfactory estimations also when a scatterer is buried beneath the air/medium interface, especially when the medium is lossy or the measurement

aperture is slid so that the buried object is no more below it.

For the case of a homogeneous half space, the proposed procedure does not require a medium model. Hence, estimation can be achieved without the use of a fitting scheme. Furthermore, it works without a cooperative target that would be needed in some autofocusing estimation procedures. Finally, the proposed procedure is extremely quick, almost real time after data collection, even though it must be run for each adopted frequency. However, the estimation procedure requires the knowledge of the antenna plane-wave spectra. Such spectra could be difficult to obtain when antenna are in close proximity to the air/medium interface as mutual coupling cannot be negligible. Therefore, to tackle such a problem further efforts must be made. A first preliminary way to solve that problem is described in [19] where a simple time-gating procedure is proposed.

Finally, a two-layered half-space medium has been addressed as well. In this case, we have shown that the estimation of the reflection coefficient is “sufficiently good” to be used in a subsequent optimization stage to infer medium’s parameters.

REFERENCES

1. Persico, R. and F. Soldovieri, “Effects of uncertainty on background permittivity in one-dimensional linear inverse scattering,” *Journal of the Optical Society of America, Pt. A.*, Vol. 21, 2334–2343, 2004.
2. Hasar, U. C., “Permittivity measurement of thin dielectric materials from reflection only measurements using one-port vector network analyzers,” *Progress In Electromagnetics Research*, Vol. 95, 365–380. 2009.
3. Case, J. T., S. Peer, E. Gallaher, and R. Zoughi, “Microwave reflection properties of concrete periodically exposed to chloride solution of 3% Salinity and compression force,” *IEEE Trans. Instrum. Meas.*, 1000–1004, 2004.
4. Moradi, G. and A. Abdipour, “Measuring the permittivity of dielectric materials using STDR approach,” *Progress In Electromagnetics Research*, Vol. 77, 357–365, 2007.
5. Frolik, J., “On the feasibility of impulse reflection response data from onedimensional multilayered lossy media,” *IEEE Trans. Antennas Propag.*, Vol. 51, 184–194, 2003.
6. Mikhnev, V. A. and P. Vainikainen, “Two-step inverse scattering method for one-dimensional permittivity profiles,” *IEEE Trans. Antennas Propag.*, Vol. 48, 293–298. 2000.
7. Uno, T. and S. Adachi, “Inverse scattering method for

- one dimensional inhomogeneous layered media," *IEEE Trans. Antennas Propagat.*, Vol. 35, 1456–1466, 1987.
8. Ghodgaonkar, D. K., V. V. Varadan, and V. K. Varadan, "Free-space measurement of complex permittivity and complex permeability of magnetic materials at microwave frequencies," *IEEE Trans. Instrum. Measur.*, Vol. 39, 387–394, 1990.
 9. Brancaccio, A., F. Soldovieri, G. Leone, D. Sglavo, and R. Pierri, "Microwave characterization of materials in civil engineering," *Proceedings of the European Microwave Association*, Vol. 2, 128–135, 2006.
 10. Minet, J., S. Lambot, E. C. Slob, and M. Vanclooster, "Soil surface water content estimation by full-waveform GPR signal inversion in the presence of thin layers," *IEEE Trans. Geosc. Rem. Sens.*, Vol. 48, 1138–1150, 2010.
 11. Roy, J. E., "Values of effective complex permittivity of corrugated slabs computed by bistatic inverse scattering," *Proc. of IEEE Antennas and Propagation Society International Symposium (APSURSI)*, 2010.
 12. Solimene, R., G. Prisco, and F. Soldovieri, "GPR based soil electromagnetic parameters determination for subsurface imaging," *Advances in Geosciences*, Vol. 19, 39–44, 2008.
 13. Solimene, R., G. Prisco, and F. Soldovieri, "A soil estimation procedure for subsurface imaging purposes," *Proceedings of the 5th IWAGPR*, Granada, Spain, 2009.
 14. Soldovieri, F., A. Brancaccio, G. Prisco, and G. Leone, "Characterization of ultra-wideband bow-tie antennas for ground penetrating radar systems," *Microwave Journal*, Vol. 49, 186–194, 2006.
 15. Bertero, M. and P. Boccacci, *Introduction to Inverse Problems in Imaging*, IOP, Bristol, UK, 1998.
 16. Slepian, D. and H. Pollak, "Prolate spheroidal wave functions, fourier analysis and uncertainty I," *Bell Syst. Tech. J.*, Vol. 40, 43–64. 1961.
 17. Solimene, R., G. Leone, and R. Barresi, "Localizing a buried planar perfect electric conducting interface by multi-view data," *J. Opt. A: Pure Appl. Opt.*, Vol. 10, 015010-1–015010-11, 2008.
 18. Daniels, D. J., *Ground Penetrating Radar*, IEE Radar, Sonar and Navigation, UK, 2004.
 19. Solimene, R., A. D'Alterio, and F. Soldovieri, "Half-space estimation by time gating based strategy," *Proc. of GPR*, Lecce, Italy, 2010.